EARTH'S CRYOSPHERE
SCIENTIFIC JOURNAL

Earth`s Cryosphere, 2017, vol. XXI, No. 1, pp. 86–96 **http://earthcryosphere.ru/**

METHODS OF CRYOSPHERE'S RESEARCHES

DOI: 10.21782/EC2541-9994-2017-1(86-96)

CHANGES TO TUNDRA LAND COVER IN FIRE-AFFECTED AREAS: *LANDSAT*-BASED STUDIES

S.G. Kornienko

Oil and Gas Research Institute, RAS, 3, Gubkina str., Moscow, 119333, Russia; spaceakm2@ogri.ru

Typical trends in spectral indices and land surface temperature in fire-affected tundra areas within the Urengoy oil and gas condensate field have been studied using *Landsat* imagery for the period from 1987 to 2014. The recovery time for the land cover thermal regime estimated according to long-term changes of land surface temperatures is much longer than for surface albedo, emissivity, and spectral indices. Other types of landscape changes in extensively burned areas can be estimated only by interpreting comprehensively the dynamics of land cover parameters calculated from spaceborne data.

Albedo, satellite images, emissivity, fire, land cover, land surface temperature, tundra

INTRODUCTION

Changes in heat transfer across the permafrost-air interface, specifically in disturbed natural moss-lichen-shrub-grass tundra land cover [*Ershov, 2004*], may trigger hazardous geological processes. Removal of land cover, by clearing or burning, interferes with the temperature regime and thaw depths [*Skryabin and Varlamov, 2013*]. Land cover occupies 90–95 % of the surface area in southern tundra and forest tundra (without water body areas). Reindeer lichen (Cladonia) dries out on warm sunny days and may burn in fires which are often triggered by industrial or household activities. Fires have destroyed land cover over at least 14 % of the territory in the Taz Peninsula for thirty years since the onset of petroleum exploration and production [*Kornienko, 2011*]. High land cover moisture, in the presence of abundant lakes, rivers, and small streams, maintains regrowth of grass, shrub, and moss vegetation in fire-affected areas, but the regrown land cover may suffer from repeated fires, as it has been observed lately, e.g., at the Urengoi oil-gas-condensate field.

Changes to landscapes (and permafrost) as a consequence of fires can be successfully evaluated using satellite remote sensing, especially in the optic waveband, which provides broad coverage, high resolution, and sufficient periodicity of observations [*Westermann et al., 2011; Loboda et al., 2013; Brooker et al., 2014; Beck et al., 2015; Muster et al., 2015*]. The experience of using spaceborne data for detecting and exploring landscape changes and causes of temperature variations is of special importance. Some difficulty may arise in detection of soil moisture changes within zones of disturbed land cover. The reliability of such results can be improved by means of multi-parametric modeling of landscape changes, where each parameter represents certain properties of the land surface.

In this study the multi-parametric approach is implemented using processed and interpreted archive *Landsat* imagery to study the recovery of the tundra land cover at fire-affected sites.

PROCESSING AND INTERPRETATION OF SATELLITE IMAGES: JUSTIFICATION OF THE METHOD

The radiation budget of the Earth's surface, with changing solar energy fluxes, is [*Ershov, 2004*]

$$R = Q(1 - A) - (E_n - E_a),$$

where Q is the total solar energy including the received and backscattered components; A is the land surface albedo; E_n and E_a are the outgoing and incoming long-wave radiation from and to the surface, respectively; the outgoing radiation found by the Stefan–Boltzmann law is

$$E_n = \varepsilon\delta T_s^4,$$

where ε is the surface spectral emissivity; δ is the Stefan-Boltzmann constant, $\delta = 5.67 \cdot 10^{-8}$ W/(m^2·K^4); T_s is the skin temperature of the Earth surface (or land surface temperature), K.

If the insolation, atmosphere transmission, and weather conditions are assumed to be invariable within the study area at the time of shooting ($Q = E_a$ at any point), R will depend on A and ε, which refer to the surface properties, and T_s controlled by the temperature of the active layer, including the land cover. Burning of land cover leads to abrupt decrease in A and ε and increase in T_s as the land surface receives more and returns less heat, and soil moisture reduces as well. Vegetation regrowth in burned areas, on the contrary, increases A and ε but reduces T_s, which may be used as indicators of ecological succession initiated by the fire disturbance. It is possible to calculate A, ε and T_s from multiband satellite remote sensing data, including *Landsat* imagery.

Scenes of different dates are inevitably shot under different conditions of insolation, transmission, and weather, which deteriorates the quality of long-term A, ε, and T_s variations in fire-affected areas estimated from spaceborne data. Therefore, it is reasonable to obtain relative estimates: to study time-dependent variations in difference between absolute values of parameters at adjacent burned and unburned sites presumably exposed to the same atmospheric conditions. The quality of the results can be further improved by bringing these conditions to the same level during preprocessing of the whole temporal stack of satellite images.

In this study, the land cover changes have been assessed using *NDVI*, *NBR* and *NDWI* spectral indices besides the A, ε, and T_s parameters. *NDVI* (Normalized Difference Vegetation Index) sensitive to the contents of chlorophyll is an indicator of vegetation abundance [*Tucker, 1979*]; *NBR* (Normalized Burn Ratio) is a proxy of fire extent and burn severity of vegetation [*Loboda et al., 2013*]; and *NDWI* (Normalized Difference Water Index) refers to land cover moisture [*Gao, 1996*]. Being sensitive to moisture content, *NBR* and *NDWI* have implications for the vulnerability of land cover to fire hazard.

The recovery time is counted from the fire event to the point of complete succession (climax) of vegetation: a moss-grass-shrub land cover that commonly regrows in the place of burnt mainly lichen cover. Correspondingly, the parameters are considered as recovered when they stop changing by post-fire succession. In the suggested approach, the variations and recovery times of the parameters at fire sites are differential estimates relative to the respective values at undisturbed reference sites.

The land surface albedo is found as [*Liang, 2000*]

$$A = 0.356\rho_1 + 0.130\rho_3 + 0.373\rho_4 + 0.085\rho_5 + \\ + 0.072\rho_7 - 0.0018,$$

where $\rho_1, ..., \rho_7$ is the spectral radiance in visible, near-infrared, and medium-infrared Thematic Mapper (TM) and Enhanced TM Plus (ETM+) images of *Landsat* 5 and 7 satellites. Albedo (from 0 to 1) is estimated from *Landsat* 8 data using identical bands 2, 4, 5, 6 and 7 of the OLI radiometer. The values of *NDVI*, *NBR* and *NDWI* (from –1 to 1) are estimated as

$$NDVI = \frac{\rho_4 - \rho_3}{\rho_4 + \rho_3}, \quad NBR = \frac{\rho_4 - \rho_7}{\rho_4 + \rho_7}, \quad NDWI = \frac{\rho_4 - \rho_5}{\rho_4 + \rho_5}.$$

from *Landsat* 5 and 7 data; *Landsat* 8 data are used in the same way but with bands 4, 5 and 6 instead of 3, 4 and 5. The emissivity ε (0 to 1) is given by [*Van de Griend and Owe, 1993*]

$$\varepsilon = 1.0094 + 0.047 \ln (NDVI).$$

The land surface temperature T_s is calculated as [*Weng et al., 2004*]

$$T_s = \frac{T_r}{1 + \left(\lambda T_r / k\right) \ln \varepsilon},$$

where T_r is the radiative surface temperature measured by satellite thermal sensors: band 6 of the *Landsat* 5 and 7 TM and ETM+ instruments and 10 of the *Landsat* 8 TIRS radiometer; λ is the thermal band wavelength; k is constant ($1.438 \cdot 10^{-2}$ m·K). Note that all T_s values and their variations are quoted in °C in the results.

Land cover changes were studied using *Landsat* scenes of 20.07.1987, 15.07.1988, 03.08.1989, 12.07.1990, 07.08.1999, 25.07.2009, 20.07.2013, and 15.08.2014 acquired in the central part of the Urengoy oil-gas-condensate field, with a resolution of 30 m in the visible, near-infrared, and medium-infrared wavebands and a lower resolution of 60, 100 or 120 m (depending on satellite number) in far-infrared (thermal) bands. Only clear-sky scenes were selected, which were shot on dates the closest to the mid-summer time. Weather information for the acquisition date and a few days before it was checked additionally to avoid distortions by heavy rainfall or strong wind events, which affect especially the thermal-band data.

The preprocessing procedure included all radiometric calibrations, geometric correction, and reprojecting the images to UTM projection (WGS-84). The selected scenes were processed with the *ENVI 4.8* software.

As noted above, long-term trends of parameters inferred from spaceborne data inevitably bear errors caused by difference in the conditions of insolation, transmission, and weather, as well as by phenological changes in vegetation and spectral band calibration. Among the weather conditions, air temperature at the time of shooting is the strongest control. To reduce these effects, various corrections are applied to time series of satellite data [*Zhu and Woodcock, 2014; Shen et al., 2016*].

All factors jointly can change the differential and average values of each parameter (multiplicative and additive components, respectively). The differential values are corrected using a linear regression equation relating the reference and corrected scenes [*Shen*

et al., 2016]. In our case, the scenes of 1987 were used for reference while all others were corrected data. The regression coefficients were calculated from average values of parameters over groups of reference undisturbed sites (easily deciphered sand bars, open larch woodlands in floodplains, areas of primary shrub-lichen vegetation, or sparse larches growing on lichen cover). Each group comprised sites with the most proximal spectral characteristics.

The T_s estimates were corrected with the same procedure as other parameters because random or periodic air temperature variations lead to changes in differential and average values of land surface temperature due to the thermophysical heterogeneity of land cover [*Westermann et al., 2011*]. Since the correction levels out average (background) values of parameters for unburned areas, this approach is applicable only to local landscape changes while the global or regional trends are removed.

STUDY AREA

The study area covers about 280 km^2 in the subarctic forest tundra, at the Arctic Circle latitude. The values of parameters used as proxies of the land cover state were compared between burned and unburned areas (Fig. 1). All sites (except for No. 5) are located near the Ngarka-Tab'yakha River floodplain and belong to the same landscape type of relatively well drained glacial lake plains, with elevations 60–70 m above sealevel. The land cover of the area includes sparse birch and larch woodlands, shrubs, moss and lichen vegetation growing on differentiated gley tundra or locally sod-podzol gley soils, mainly of

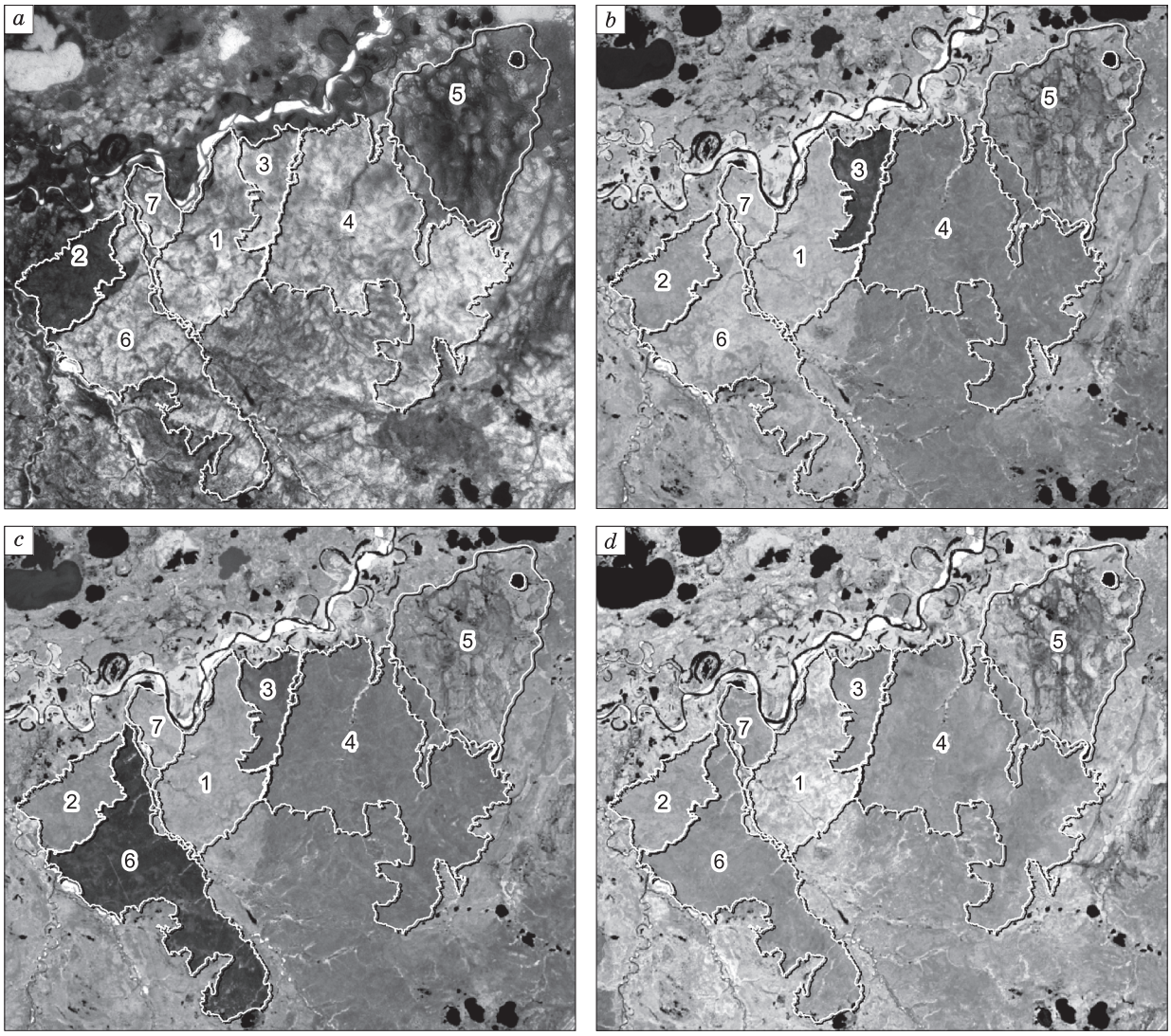

Fig. 1. Satellite images of sites 1–7 within the Urengoy oil-gas-condensate field: KFA-1000 (*a*), *Landsat* 5 (*b*, *c*), and *Landsat* 8 (*d*) scenes shot in September 1979 (*a*) and on 20.07.1987 (*b*), 03.08.1989 (*c*), and 15.08.2014 (*d*).

sand, silt, and clay silt lithologies. Site No. 5 is generally a plain with low hills and abundant lakes, at elevations 45–55 m asl. There are widespread raised bogs with flat mounds and yernik-ledum-sphagnum vegetation, shrubs, mosses, and sporadic birch-larch woodlands that grow on tundra gley and muddy humus-rich soils (mainly clay silt, silt, and peat).

The land cover before fire events is imaged in a panchromatic scene (Fig. 1, *a*) shot on September 1979 by a KFA-1000 camera placed on a Russian satellite. Site No. 1, 10.1 km^2, belongs to the unburned area, with a mainly lichen-shrub land cover (Fig. 2, *a*). Another undisturbed reference site (No. 2), 6.4 km^2, is grown with open larch woodlands over the lichen cover (Fig. 2, *b*), with dwarf birch, ledum, blueberries, and bilberries in the undergrowth. Site No. 5 occupies 22.2 km^2 in a swampy area, with a prominent dense network of creeks (Fig. 1). Variations in spectral indices and land surface temperature at fire sites 3, 4, 6 and 7 were estimated relative to the respective values for the reference sites 1 and 2. According to the available spaceborne data, 7.5 km^2 site No. 3 burned before 20 July 1987 (Fig. 1, *b*) and site No. 4 (25.3 km^2) was affected by an extensive fire

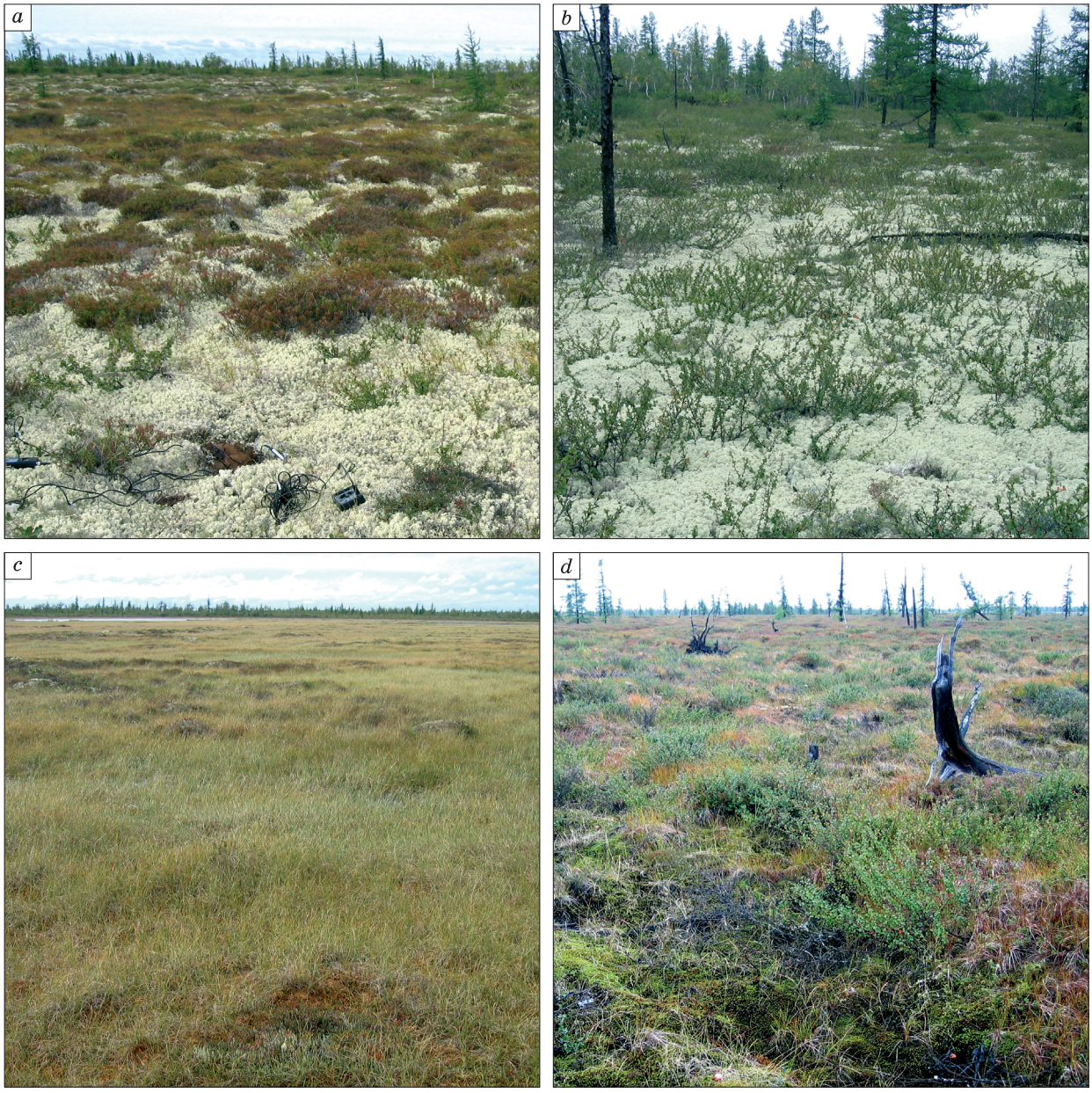

Fig. 2. Primary land cover at sites 1 (*a*) and 2 (*b*); secondary land cover at a site similar to No. 1, 22 years after a fire (*c*); secondary land cover at a site similar to No. 2, 10 years after a fire (*d*).

about 1983, while site No. 6 (16.3 km^2) burned in 1989 (Fig. 1, *c*); a fire event at 4.4 km^2 site No. 7 occurred between 1994 and 1997.

As imaged by the scene of 1979 (Fig. 1, *a*), the land cover at all sites affected subsequently by fires was the same as at site 1 (Fig. 2, *a*). See, for instance, one such site in Fig. 2, *c*: its land cover prior to a fire event of 22 years ago was similar to that of site 1; the regrown vegetation at the site consists of moss, grass, and shrubs. The photograph of Fig. 2, *d* illustrates ecological succession 10 years after a fire at a site that had the same primary land cover as at site 2 (Fig. 2, *b*).

INTERANNUAL VARIATIONS IN SPECTRAL INDICES AND LAND SURFACE TEMPERATURE AT FIRE-AFFECTED SITES

Interannual variations of parameters after all corrections were plotted as average values (means)

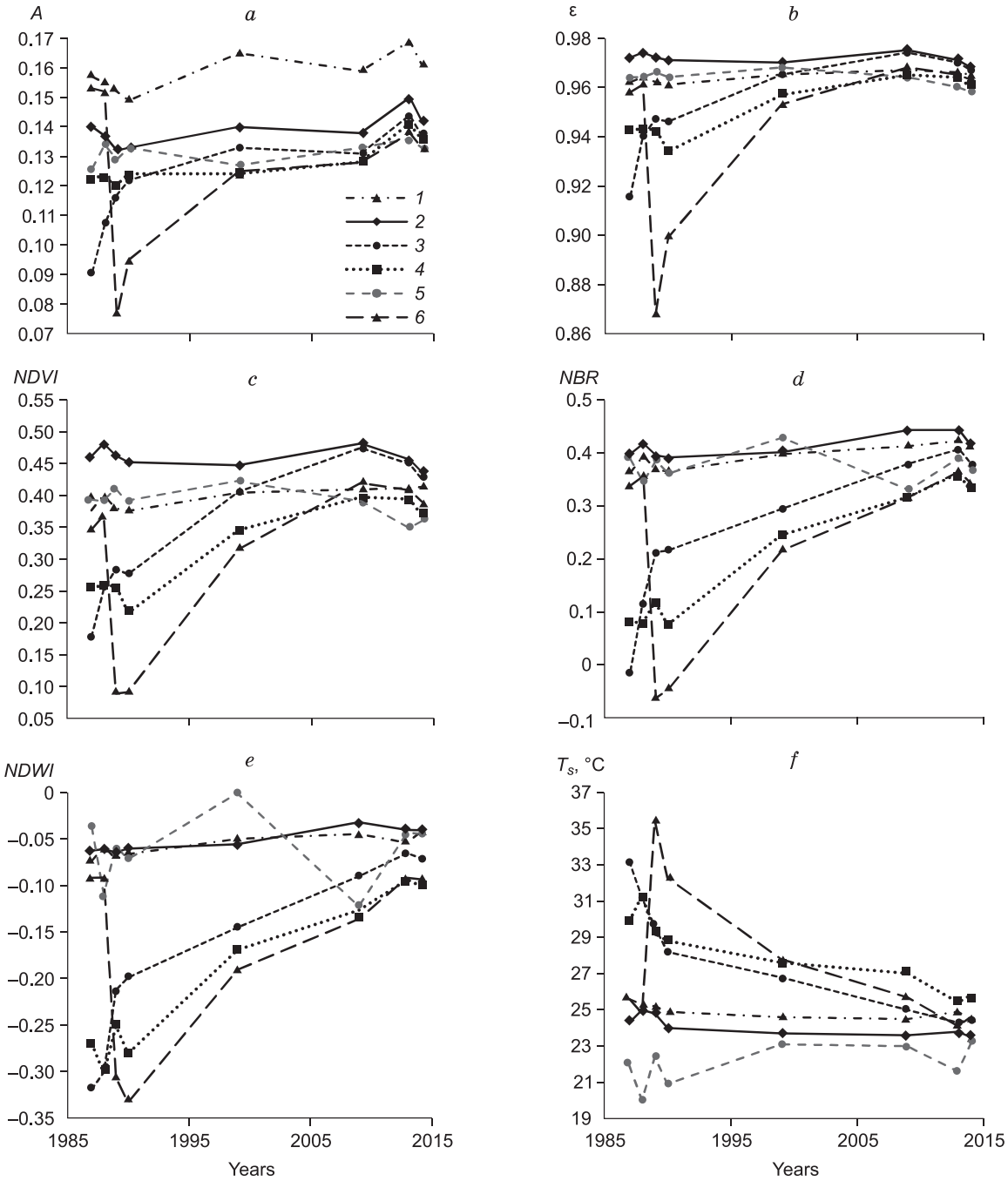

Fig. 3. Time-dependent variations in parameters means at sites 1–6 for 1987 through 2014:
albedo, *A* (*a*), emissivity, ε (*b*), *NDVI* (*c*), *NBR* (*d*), *NDWI* (*e*), land surface temperature, T_s (*f*).

vs. time for all sites, except No. 7 (Fig. 3). All parameters decreased dramatically after fires while T_s became 8–10 °C higher. The variations were the smallest at reference sites (Nos. 1 and 2); at site No. 5, they were large but random, most likely, because of hydrological variations in the swampy terrain. All curves for fire-affected sites obviously approached the reference values by the end of the observation period. Although site 4 burned earlier than all others, its parameters recovered more slowly than those for sites 3 and 6.

Different parameters within the same sites have different recovery times (Fig. 3). Specifically, albedo and emissivity recover faster than other parameters. In order to characterize the rate and time of land cover changes at burned sites using differential parameter means with respect to adjacent undisturbed sites, reference was made to site No. 2, where variations in the values of parameters and their RMSD (standard deviation or one-sigma error) were the smallest. Thus, time-dependent difference was calculated between parameter means at reference site 2 and at sites 3 and 6, for which the fire dates were known. Then approximation equations were found for the differential values that represented long-term trends (Fig. 4). Interannual variations of RMSD (Fig. 5) in-

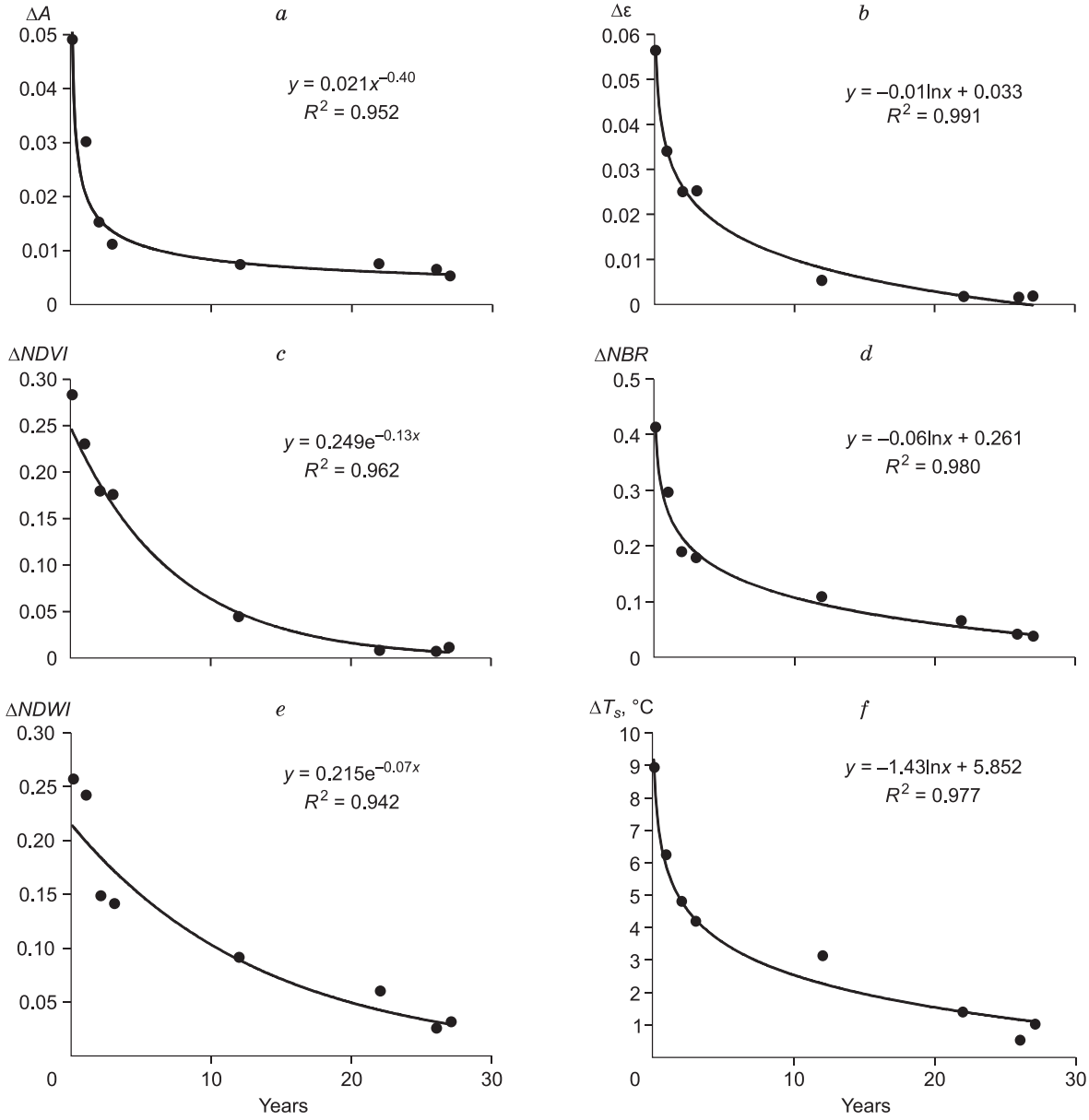

Fig. 4. Time-dependent variations in differential parameter means at site 3 relative to site 2:
albedo, *A* (*a*), emissivity, ε (*b*), *NDVI* (*c*), *NBR* (*d*), *NDWI* (*e*), land surface temperature, T_s (*f*).

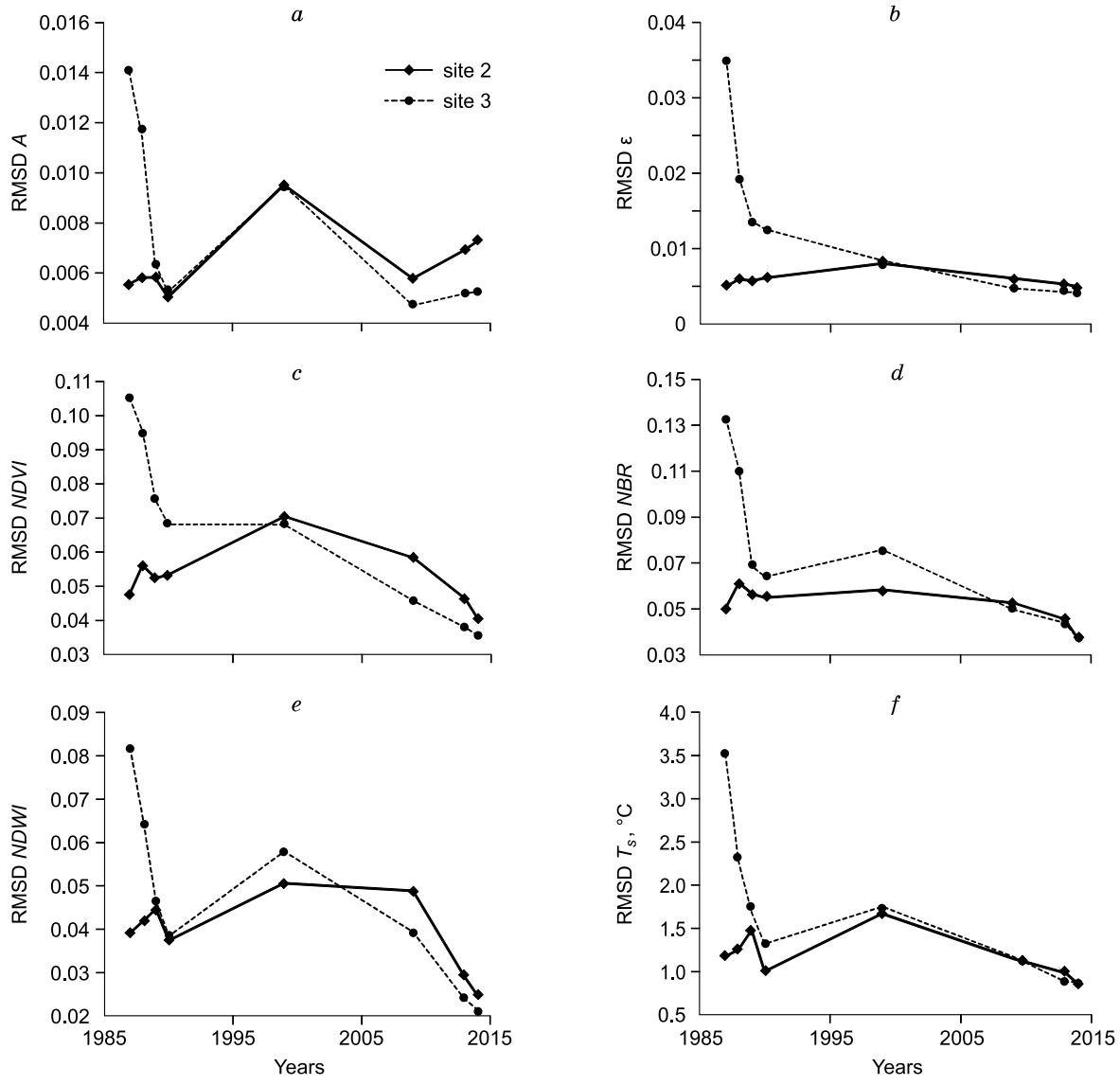

Fig. 5. Time-dependent variations in RMSD of parameter means at site 3 relative to site 2 for 1987 through 2014:

albedo, *A* (*a*), emissivity, ε (*b*), *NDVI* (*c*), *NBR* (*d*), *NDWI* (*e*), land surface temperature, T_s (*f*).

Table 1. **Recovery times for different parameters (years)**

Parameter	Site 3 with respect to site 2		Site 6 with respect to site 2	
	Average parameter values	RMSD	Average parameter values	RMSD
A	5.8	12.6	14.7	17.0
ε	13.8	10.6	15.7	13.4
NDVI	14.3	18.3	17.7	17.8
NBR	16.4	11.0	19.3	18.8
NDWI	19.8	8.0	20.3	16.9
T_s	22.4	9.2	24.3	15.7

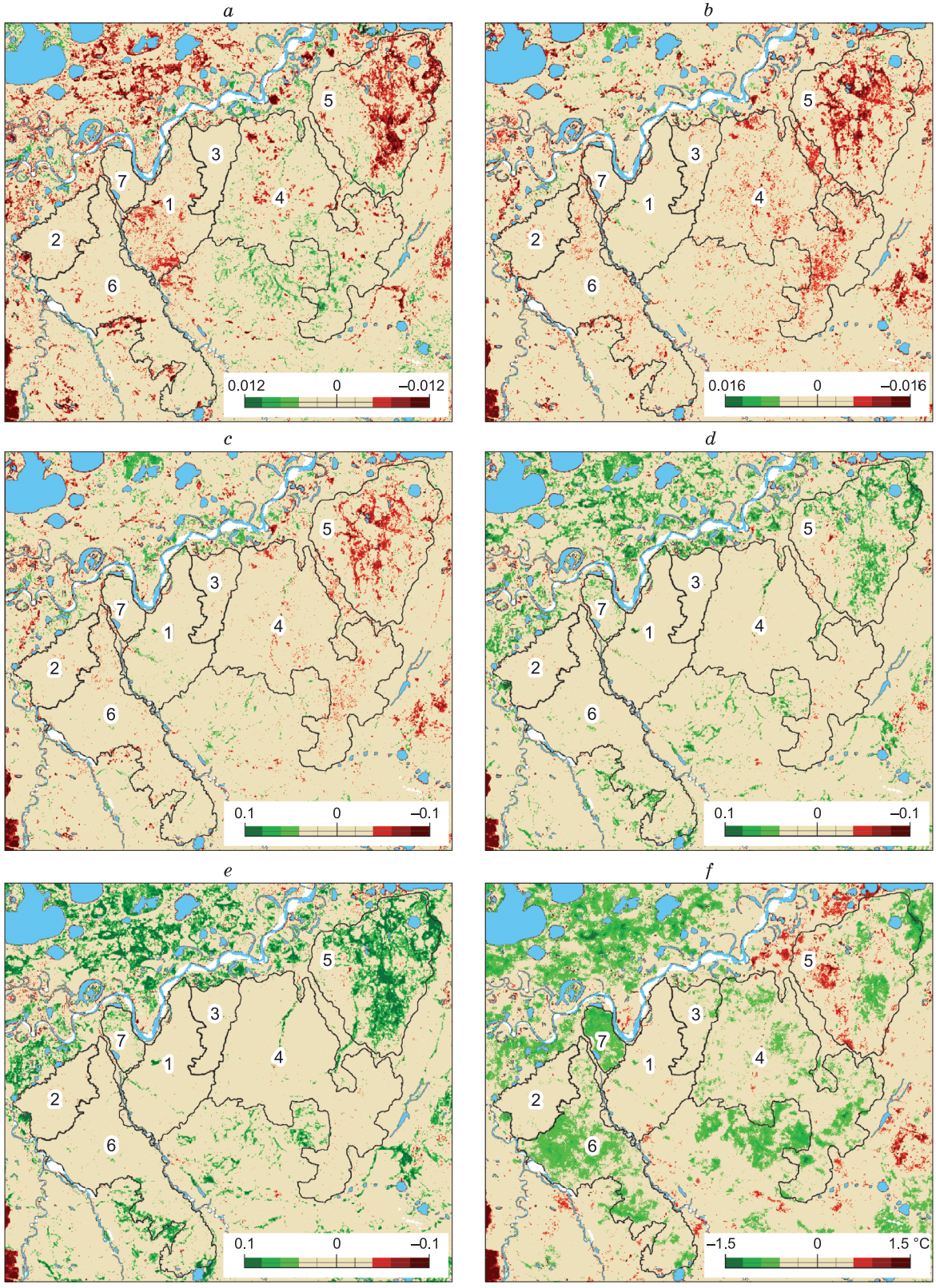

Fig. 6. Maps showing relative variations of parameters in the study area for 2009 through 2014:
albedo, *A* (*a*), emissivity, ε (*b*), *NDVI* (*c*), *NBR* (*d*), *NDWI* (*e*), land surface temperature, T_s (*f*).

Table 2. **Percentages (%) of area free from signatures of ongoing succession at fire sites for the period 2009–2014**

Site	Parameter					
	A	ε	*NDVI*	*NBR*	*NDWI*	T_s
3	99.65	100	99.97	99.75	99.60	92.50
4	94.86	99.99	99.77	99.21	99.15	83.40
6	99.27	99.84	99.53	96.64	95.15	63.08
7	98.97	99.83	98.87	88.01	87.43	21.89

creased abruptly after the fire events and then decreased slowly, at similar rates, for all parameters. Regression equations for differential RMSD for fire sites with respect to those at site 2 were obtained in the same way as for the yearly variations of differential parameter means.

The recovery rates were compared using a criterion showing the time required for the difference of parameter means and their RMSD from the respective background values to reduce for 90 % of the total range (the total range is the maximum difference minus the minimum one). The recovery times were estimated using approximation equations based on field data. Table 1 lists recovery times for different parameters at sites 3 and 6 calculated as 90 % reduced difference relative to the background values at reference site 2.

Alternatively, the recovery times for the spectral indices of land cover at burned sites can be compared as relative percentages of site surface areas with and without changes in parameter values for certain observation periods. Figure 6 shows maps of parameter changes for the past 5 years, as difference in parameter distributions between 2014 and 2009. All parameter changes are given with respect to the background of site 2, where the average difference of values was assumed to be zero: a datum against which parameter changes were estimated for fire sites and for the study area as a whole. The zones of background values (no change, beige color in Fig. 6) were outlined according to the interannual variations of parameters at site 2, within 99 % confidence interval. The ranges in the color-coded scales correspond to units in which the parameters are measured.

Green color shows zones where all parameters increased (T_s decreased) indicating current succession. Red color corresponds to decrease of all parameters (T_s increase) which must be due to causes other than succession at previously disturbed sites, because no signs of repeated fires were observed. Thus, beige and red zones in Fig. 6 are free from signatures of ongoing ecological succession (Table 2). All parameter values were likewise estimated within 99 % confidence interval.

DISCUSSION

The analyzed parameters show markedly different recovery times (Table 1): the albedo, which is normally high in bare soil (sand and silt in our case), recovers the fastest, while the recovery of land surface temperature takes the longest time. The recovery times predicted for the parameters at sites 3 and 6 differ, possibly, because site 3 burned two years earlier than site 6 and data were acquired at different periodicity after the fires. Nevertheless, the recovery times generally increase from the shortest for *A* to the longest for T_s at both sites. The recovery time for T_s RMSD is commensurate with that for other parameters, which means that the spectral and thermophysical properties of the land cover become less heterogeneous at similar rates as its recovery progresses.

Maps in Figure 6 and data in Table 2, which show the dynamics of the parameters for the past 5 years of observations (second criterion), are generally consistent with estimates according to the first criterion (Table 1). At site 3, the values of all parameters, except T_s, became stable (vegetation regrowth has been complete) over more than 99 % of the area (92.5 % for T_s, Table 2) twenty two years after the fire. At site 6, T_s recovered over 63 % of the site area only in twenty years after the fire, when other parameters stopped changing. If the fire event at site 7 occurred no later than 1994, the recovery time would be 15 years for *A*, ε and *NDVI* (99 % of the area), but T_s has reached the initial values over 22 % of the area only for this time. Unlike sites 3 and 6, the *A* and T_s values at site 4 recovered over ~95 % and 83.4 % of the area, respectively, twenty six years after the fire. The recovery times for *NBR* and, especially, *NDWI*, sensitive to soil moisture, are longer than for *A*, ε and *NDVI* but shorter than for T_s.

Field surveys of 2005 and 2006 at sites of old fires and succession processes within the studied territory, compared with dates of fires according to archive satellite images, indicate that vegetation regrowth can become complete in ~20 years (Fig. 2). These estimates generally agree with data from Tables 1 and 2, except for T_s, which takes at least 25–30 years to recover. Thus the radiation budget will

recover in approximately 25–30 years from the fire to the point when its variations will no longer result from succession. The T_s difference between reference sites 1 and 2 remained almost the same, for the previous 24 years (Fig. 3) and for the past five years of observations (Fig. 6).

The longer T_s recovery time in fire-affected areas and continuing cooling of the land cover surface after complete vegetation regrowth may be due to accumulation of heat in the soil and elevated mean annual ground temperatures after fires. Removal of the moss-lichen cover is known to cause permafrost warming [*Ershov, 2004*]. For instance, the ground temperature at the depth 20 cm in a disturbed frost heave (devoid of vegetation) was reported [*Melnikov, 2012*] to be always warmer than in a similar heave which preserved its cover. Sphagnum over permafrost makes its mean annual temperatures 0.5 to 1.5 °C colder in tundra and 2–3 °C colder in forest tundra and northern taiga; cooling under moss and lichen in forest tundra is 0.5–1.0 °C [*Ershov, 1989*]. On the contrary, the ground temperature at 10 m below the surface at cleared fire sites remains 1.0–1.5 °C warmer than before fires, even in 20–25 years [*Skryabin and Varlamov, 2013*]. Colder temperatures of the ground (and, hence, of the regrown vegetation surface), may also correspond to higher soil moisture and higher transpiration, to which T_s is more sensitive than other parameters. The higher land cover moisture is consistent with relatively long recovery times for *NDWI* (Table 1). At the same time, *NDWI* at site 6 changed insignificantly while T_s decreased markedly (Fig. 6, Table 2).

The quite notable difference in recovery times for the same parameters at sites 3, 4, 6 and 7 indicates possible difference in succession rates, even within a single geomorphic zone, as it was noted earlier [*Melnikov, 2012*].

The revealed trends in the behavior of parameters in burned areas allow more reliable characterization of processes in undisturbed areas. Namely, increase in *NBR* and *NDWI* at site 5 most likely results from moisture increase (Fig. 6). Greater amounts of water at the site (in land cover, in bare substrate, and in shallow lakes or pools) may also be responsible for lower *A*, *NDVI*, and ε (derived from *NDVI*) and for T_s decrease over a large part of the site. On the other hand, *A* decrease at site 1 (Fig. 6) cannot result from moisture increase because other parameters remain almost invariable. However, greater moisture may lead to *A* reduction at sites north of the Ngarka-Tab'yakha River (left top corner in the image) where *NBR* and *NDWI* became higher while T_s cooled down. These examples show that only comprehensive interpretation of changes to parameters in areas of extensively disturbed land cover can distinguish fire-initiated succession from wetting and ensure appropriate assessment of landscape changes.

Generally, the reported results demonstrate rather high information value of *Landsat* temporal stacks for characterization of land cover in fire-affected areas and for detection of changes in landscape conditions of permafrost-air heat exchange.

CONCLUSIONS

Analysis of interannual variations in parameters that represent changes in the tundra land cover in fire-affected areas inferred from *Landsat* imagery leads to the following inferences.

The recovery times for land surface temperature and radiation budget at sites of fire-induced succession reach 25–30 years and are markedly longer than those for albedo, emissivity, and spectral indices (*NBR*, *NDWI* and *NDVI*).

The recovery times for the land cover spectral indices may differ considerably within geomorphic zones of the same types which had identical land covers before the fire disturbance.

Landscape changes (including those related to moisture) in areas of extensively burned land cover and fire-initiated succession can only be characterized by comprehensive interpretation of changes to all parameters calculated from spaceborne data.

References

Beck, I., Ludwig, R., Bernier, M., Lévesque, E., Boike, J., 2015. Assessing permafrost degradation and land cover changes (1986–2009) using remote sensing data over Umiujaq, Sub-Arctic Québec. Permafrost and Periglacial Processes 26, 129–141.

Brooker, A., Fraser, R.H., Olthof, I., Kokelj, S.V., Lacelle, D., 2014. Mapping the activity and evolution of retrogressive thaw slumps by tasselled cap trend analysis of a Landsat Satellite Image Stack. Permafrost and Periglacial Processes 25, 243–256.

Ershov, E.D. (Ed.), 1989. Geocryology of the USSR. West Siberia. Nedra, Moscow, 456 pp. (in Russian)

Ershov, E.D. (Ed.), 2004. Methods of Geocryological Research. Student's Manual. Moscow University, Moscow, 512 pp. (in Russian)

Gao, B., 1996. NDWI – A normalized difference water index for remote sensing of vegetation liquid water from space. Remote Sens. Environ. 58, 257–266.

Kornienko, S.G., 2011. Assessing the transformations of natural landscapes of the Taz Peninsula using space-borne imagery. Geography and Natural Res. 1, 67–73.

Liang, S., 2000. Narrowband to broadband conversions of land surface albedo. I – Algorithms. Remote Sens. Environ. 76, 213–238.

Loboda, T.V., French, N.H.F., Hight-Harf, C., Jenkins, L., Miller, M.E., 2013. Mapping fire extent and burn severity in Alaskan tussock tundra: An analysis of the spectral response of tundra vegetation to wildland fire. Remote Sens. Environ. 134, 194–209.

Melnikov, V.P. (Ed.), 2012. Comprehensive Monitoring of Northern Taiga Landscapes in West Siberia. Geo Publishers, Novosibirsk, 207 pp. (in Russian)

Muster, S., Langer, M., Abnizova, A., Young, K., Boike, J., 2015. Spatio-temporal sensitivity of MODIS land surface temperature anomalies indicates high potential for large-scale land cover change detection in Arctic permafrost landscapes. Remote Sens. Environ. 168, 1–12.

Shen, H., Huang, L., Zhang, L., Wu, P.H., Zeng, C., 2016. Long-term and fine-scale satellite monitoring of the urban heat island effect by the fusion of multi-temporal and multi-sensor remote sensed data: A 26-year case study of the city of Wuhan in China. Remote Sens. Environ. 172, 109–125.

Skryabin, P.N., Varlamov, S.P., 2013. Ground thermal regime in disturbed landscapes of Central Yakutia. Kriosfera Zemli XVII (3), 44–49.

Tucker, C.J., 1979. Red and photographic infrared linear combinations for monitoring vegetation. Remote Sens. Environ. 8, 127–150.

Van de Griend, A.A., Owe, M., 1993. On the relationship between thermal emissivity and the normalized different vegetation index for natural surfaces. Intern. J. Remote Sensing 14 (6), 1119–1131.

Weng, Q., Lu, D., Schubring, J., 2004. Estimation of land surface temperature-vegetation abundance relationship for urban heat island studies. Remote Sens. Environ. 89, 467–483.

Westermann, S., Langer, M., Boike, J., 2011. Spatial and temporal variations of summer surface temperatures of high-arctic tundra on Svalbard – Implications for MODIS LST based permafrost monitoring. Remote Sens. Environ. 115, 908–922.

Zhu, Z., Woodcock, C.E., 2014. Continuous change detection and classification of land cover using all available Landsat data. Remote Sens. Environ. 144, 152–171.

Received September 25, 2015